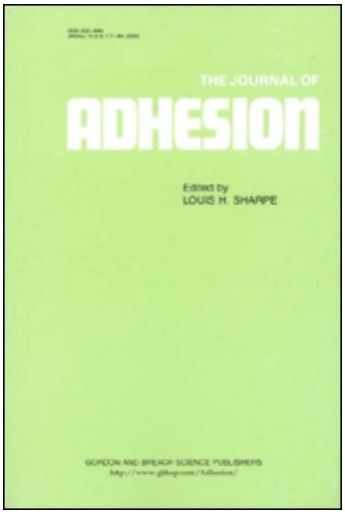

The Journal of Adhesion

Publication details, including instructions for authors and subscription information:
http://www.informaworld.com/smpp/title~content=t713453635

Studies on the Interphase of a Model Adhesive Joint

W. Possart[a]; D. Fanter[a]; S. Dieckhoff[b]; T. Gesang[b]; A. Hartwig[b]; R. Höper[b]; V. Schlett[b]; O. D. Hennemann[b]

[a] Fraunhofer-Institute for Applied Materials Research, Aussenstelle Teltow, Germany [b] Fraunhofer-Institute for Applied Materials Research, Bremen, Germany

To cite this Article Possart, W. , Fanter, D. , Dieckhoff, S. , Gesang, T. , Hartwig, A. , Höper, R. , Schlett, V. and Hennemann, O. D.(1996) 'Studies on the Interphase of a Model Adhesive Joint', The Journal of Adhesion, 57: 1, 227 — 244
To link to this Article: DOI: 10.1080/00218469608013654
URL: http://dx.doi.org/10.1080/00218469608013654

J. Adhesion, 1996, Vol. 57, pp. 227–244
Reprints available directly from the publisher
Photocopying permitted by license only

Studies on the Interphase of a Model Adhesive Joint*

W. POSSART** and D. FANTER

Fraunhofer-Institute for Applied Materials Research, Aussenstelle Teltow, Kantstrasse 55, D-14513, Germany,

and

S.DIECKHOFF, T.GESANG, A. HARTWIG, R. HÖPER, V. SCHLETT and O-D. HENNEMANN

Fraunhofer-Institute for Applied Materials Research, Neuer Steindamm 2, D-28719 Bremen, Germany

(Received November 21, 1994; in final form June 3, 1995)

Ultra-thin films of a dicyanate bisphenol A prepolymer on aluminium or silicon substrates are studied as a model for an adhesive interphase. AFM shows structural details of the films with a lateral resolution from some 10 nm up to a few microns. Substrates have to be very flat in order to obtain continuous prepolymer layers. So the aluminium roughness of a few nanometers results in a discontinuous prepolymer distribution below about 10 nm thickness while the films remain intact down to 2 nm on the smoother silicon. XPS and IR spectroscopy show that the as-prepared layers do not undergo serious chemical changes or pronounced adhesive interactions. The native silicon surface is totally inert. The cyanate group is not involved at all. The native aluminium surface induces changes both in energy and orientation of the triazine rings, however. This may be considered as an indirect hint on some adhesive interaction of the cyanurate prepolymer with the aluminium substrate but the experimental facts do not explain the adhesion mechanism in detail yet.

KEY WORDS: thin films; cyanurate prepolymer; native aluminium surface; oxidized silicon surface; atomic force microscopy; XPS; external reflection FTIR; molecular orientation and interaction

INTRODUCTION

The properties of ultra-thin polymer films receive increasing interest for a large number of technical applications. In most instances, they are part of a composite. Therefore, adhesion plays an important part for their function. Moreover, an ultra-thin film may serve as a model system for the investigation of the molecular structure and the interactions in the interphase of a polymer adhesive adhering to a solid substrate.

This was the motivation to study the properties of a series of cyanurate prepolymer layers as a function of their thickness on aluminium and on silicon, respectively.

* One of a Collection of papers honoring Jacques Schultz, the recipient in February 1995 of *The Adhesion Society Award for Excellence in Adhesion Science, Sponsored by 3M.*

Presented in part at EURADH 94, Mulhouse, France, September 12–15, 1994, a conference organized by the Section Française de l'Adhesion, division de la Société Française du Vide.

** Corresponding author.

We suppose that the organic layer exhibits a specific three-dimensional interphase extending from the substrate to the unperturbed part of the layer (further away from the substrate) in which its bulk properties are prevailing. Consequently, an interphase contribution to the signal of any spectroscopic measurement should increase with decreasing thickness of the organic layer. In this way, a change of layer thickness will help to distinguish the interphase properties from the properties of both bulk organic layer and substrate. In addition, prepolymer and substrate are characterized individually to provide a reference.

The model substrates are silicon wafers with extremely smooth surfaces and very smooth aluminium layers produced by electron beam evaporation on silicon wafers. The materials were chosen because of their relevance to adhesive bonding in microelectronics, microsystems, aviation and light weight construction. Since the samples are handled in the laboratory, both substrate surfaces bear a native oxide layer.

A prepolymer of the dicyanate of bisphenol A (DCBA) serves as a model for a curable adhesive.

Uniform prepolymer layers between about 3 nm to 100 nm thickness are prepared from a solution by spin coating or by dip coating.

Several experimental techniques have been combined for that study. Scanning Auger Microscopy (SAM) yields the lateral distribution and the local thickness of oxide and carbon contamination on the substrates. As a routine method, ellipsometry delivers the thickness data for the oxide on the substrate for each sample just before coating and after application of the prepolymer layer. Atomic Force Microscopy (AFM) provides the topography of the substrates and insight into the morphology of the coatings. Photoelectron (XPS) and external reflection IR spectra (ERIRS) contain information about orientation and energetic state of the organic molecules.

Good adhesives can be formulated on the basis of such cyanurate prepolymers.[1-3] So we should know how they work on metals. Is it the cyanate group or the triazine grouping or something else that causes adhesion? And what is the film structure?

The paper summarizes the experimental results obtained so far. It focuses on the prepolymer film immediately after preparation. The state of interpretation will be discussed and an outlook on further routes of research will be presented.

EXPERIMENTAL RESULTS

The Uncoated Substrates

On both substrates, XPS (VG Scientific ESCALAB 220i XL with monochromatized Al Kα source and low energy electron compensation of sample charging) and AES (Perkin Elmer PHI 660 SAM; focussed primary electron beam with 5 keV) detect a carbon contamination of laterally uniform (resolution *ca.* 0.1 μm) thickness. Aliphatic carbon of about 0.5 nm thickness covers the silicon wafer. The aluminium has some 0.7 nm thick contamination. In the latter case, the carbon bonds are not purely aliphatic. Angle-resolved XPS up to 80° take-off angle revealed (C—O)- and (C=O)-components that are concentrated at the interface with the Al substrate. The outermost surface region of the contamination layer consists mainly of hydrocarbon

structures. Hence, it is possible, but not certain, that the adventitious carbon reacted with the oxide. The native oxide layers beneath that contamination are also uniform. For silicon, it is SiO_2 of about 1 nm thickness.

The aluminium is not covered by a pure oxide. XPS reveals that more than 70% of the oxygen forms OH-like states. The layer thickness varies slightly from 2.7–3.4 nm. Although both substrates visually show a surface finish like an optical mirror, AFM (Digital Instruments Nanoscope III) reveals pronounced distinctions on the microscopic level. The AFM images in Figures 1 and 2 are obtained in the contact mode and give an impression of the topography. The Si wafer is flat even on the nanometer height scale. The Root-Mean-Square roughness (RMS) amounts to only 0.13 nm. The aluminium coating is less smooth. It consists of granular structures with a typical peak-to-peak roughness of about 30 nm and a RMS roughness of 5 to 10 nm depending on the evaporation batch. The aluminium granules possess diameters of 100 to 400 nm. The inclination angles of their faces vary only from 10° to 20° with respect to the mean surface plane. Consequently, adsorbing organic molecules will see a gently-shaped profile of the uniform continuous native oxide covering the aluminium metal. The inclination angles of the oxidized silicon wafers are even one order of magnitude smaller.

The Prepolymer

The cyclotrimerization reaction of the dicyanate of the bisphenol A (DCBA) was stopped at 45 mole% conversion of the cyanate groups, thus still providing a solvable material. Figure 3 presents the chemical formulae for the monomer and the oligomer structures schematically. As the chemical reaction path is well known for that system,[4] the number distribution of the molecules can be calculated with good accuracy. The

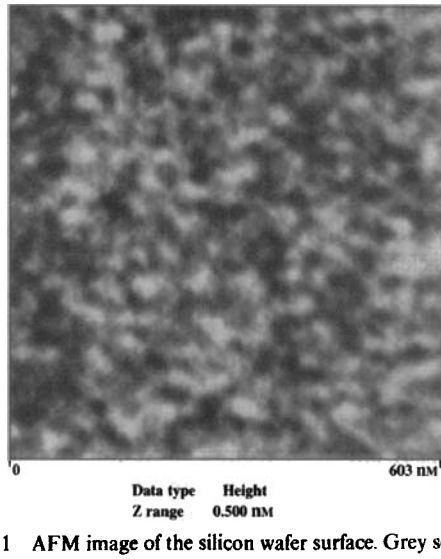

FIGURE 1 AFM image of the silicon wafer surface. Grey scale 0.5 nm.

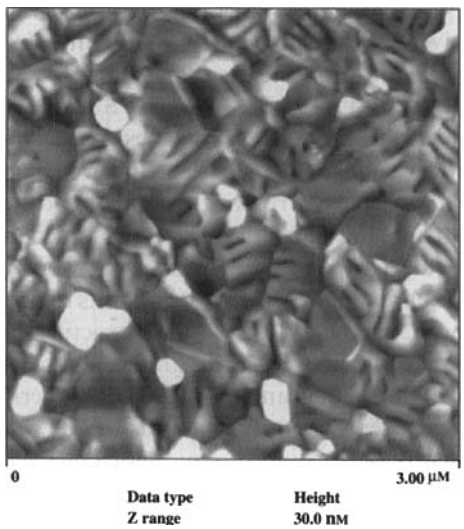

FIGURE 2 AFM image of the surface of an aluminium evaporation layer on a silicon wafer. Grey scale 30 nm.

prepolymer consists mainly of monomer DCBA and trimer molecules. Larger oligomers appear much less frequent although they dominate the weight distribution. In Figure 4, the chemical formula for the DCBA trimer reveals the manifold of different chemical environments in the prepolymer molecules.

For carbon, there exist at least five different bond states (named a–e). Both oxygen and nitrogen occur in two bond states, O_{cy}, O_{triaz} and N_{cy}, N_{triaz}, respectively.

Figure 5 shows the prepolymer core level photoelectron spectra measured at 10 eV fixed analyser transmission. Obviously, XPS resolves only three main peaks and a shake-up satellite in the Cls spectrum. The first peak to the right of the shake-up satellite stems from all carbon atoms bound to nitrogen. Mathematical curve decomposition (VG ECLIPSE 1.6m software, nonconstrained fitting of Gauss-Lorentzian lines and Tougaard inelastic background) yields the two components, C_e, C_d, assigned to the triazine ring and to the cyanate group. The components are difficult to distinguish without curve fitting. The next peak is due to those aromatic carbons, C_c and C_b, in the benzene rings that couple to the oxygen atoms. Again, spectrum decomposition provides clear distinction whether it is the cyanate group or the triazine ring in the neighbourhood. The remaining aromatic and aliphatic carbons, C_a, give rise to the most intense peak at the low-energy end of the Cls spectra. The two nitrogen bond states are not resolved in the Nls spectra at all. Fortunately, the two oxygen states are well separated in the Ols signal. Hence, the Ols spectra provide unambiguous information about the state of cyanate groups and of the triazine rings. The silicon oxide peak in the Ols spectrum stems from a contamination of the prepolymer bulk which is introduced during the powderization in a mill after synthesis.

As we expect from the multitude of structural elements in the prepolymer, the infrared spectrum is rich with bands. For illustration, Figure 6 shows a transmittance

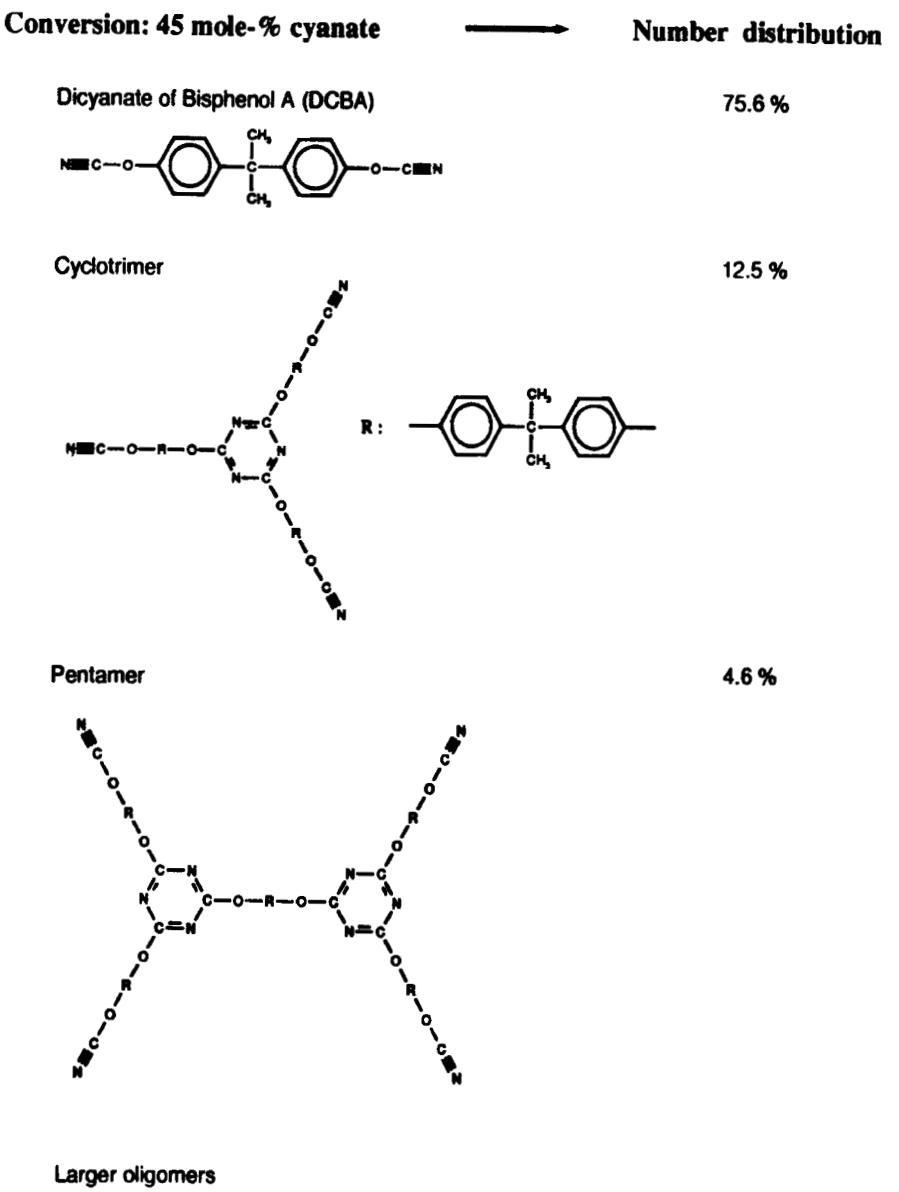

FIGURE 3 Part of the prepolymer number distribution and chemical formulae for the DCBA monomer and the first oligomers in the prepolymer.

spectrum measured on a Nic 740 (Nicolet) FTIR spectrometer. The characteristic group frequencies are identified in accordance with the literature[5–8] and the usual catalogues for IR spectra.[9–11] Hence, the assignment rests upon analogy with known similar substances and the concept of localized vibration modes. This commonly

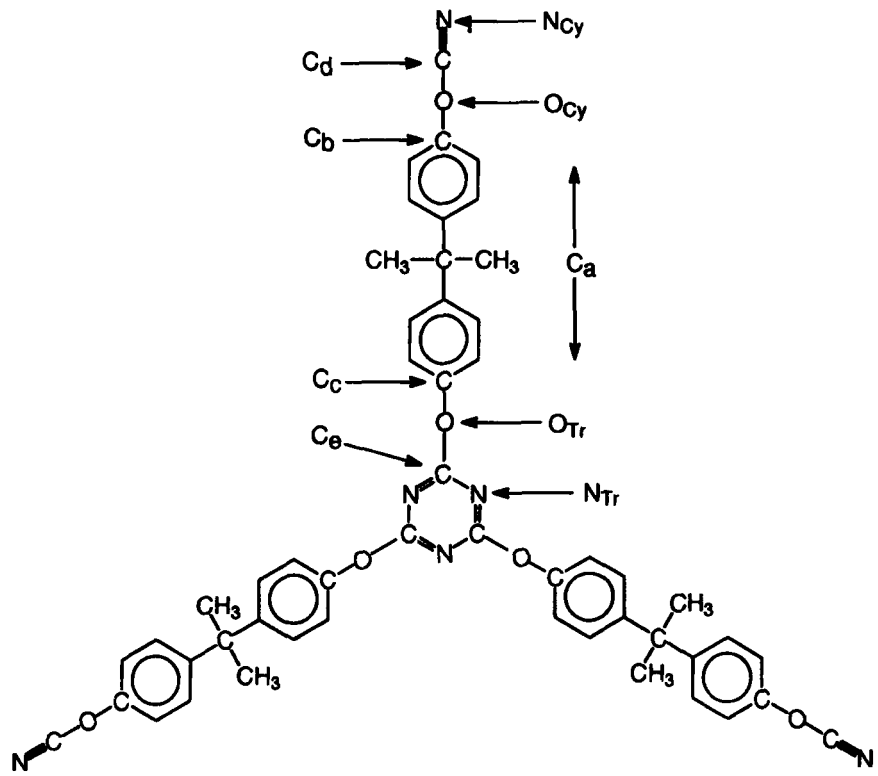

FIGURE 4 The different chemical environments in DCBA and its trimer.

adopted approach is rather qualitative. The detailed type of the molecular vibrations remains widely unspecified. In particular, this is true for the triazine ring and the cyanate group. In addition, ATR IR spectroscopy provides high quality spectra for calculating the optical function $n^*(\tilde{\nu}) = n(\tilde{\nu}) - i \cdot k(\tilde{\nu})$ ($\tilde{\nu}$ = wavenumber) of the prepolymer. The ATR spectra are taken with s-polarized light at 45° on a germanium single reflection crystal mounted in a SEAGULL reflection accessory (Harrick) for a FTS 60B (BioRad) FTIR spectrometer. The deduced optical function was utilized to recalculate the ATR spectrum. The result fits very well to the measured spectrum. The band positions are equal and the band heights are reproduced with 2–5% error. This proves that both the calculation procedure and the prepolymer optical function are well suited for the further discussion. The bulk optical function of the prepolymer will play an important role in the interpretation of the external reflection IR spectra of thin films.

Ultra-Thin Prepolymer Coatings

Now, the behaviour of the ultra-thin layers can be considered immediately after preparation in reference to the established bulk features of substrate and prepolymer.

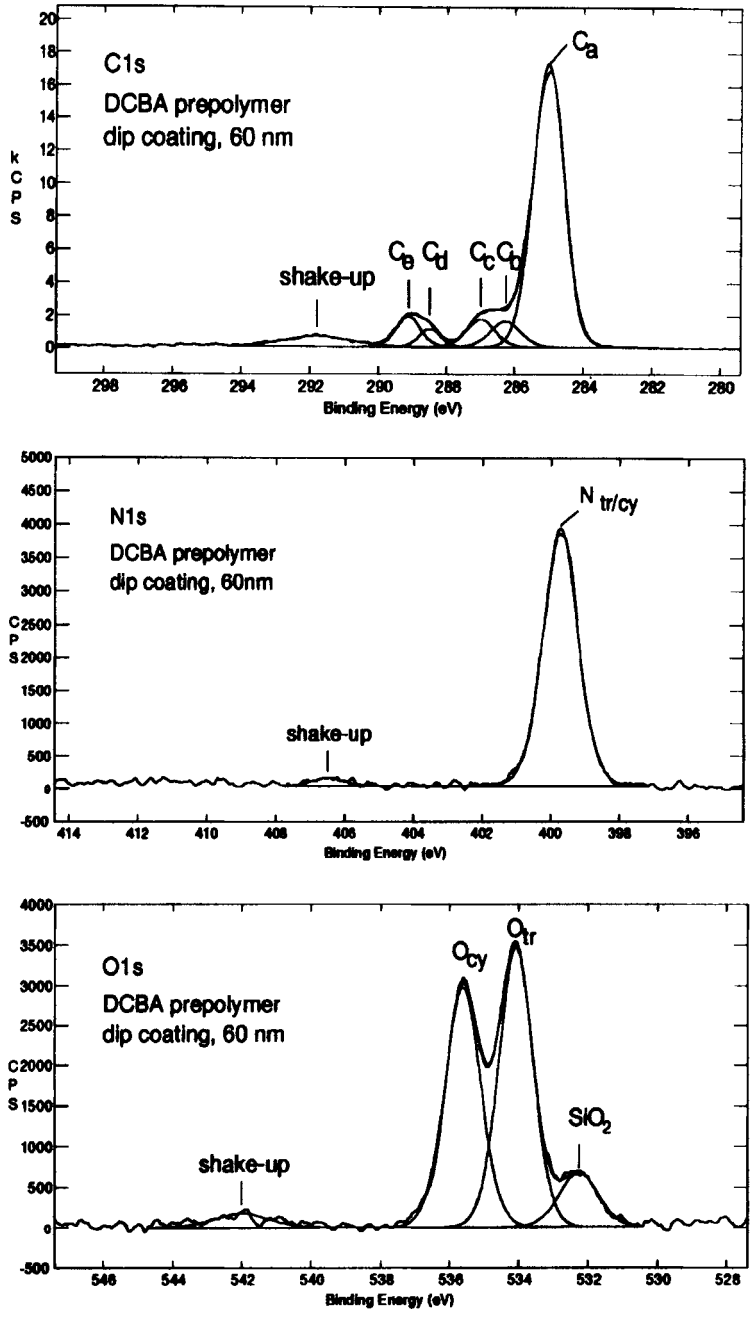

FIGURE 5 Core level photoelectron spectra measured at 60 nm prepolymer thickness on aluminium substrate. The experimental data are very well fitted by the sum curve obtained from a mathematical deconvolution into spectral components. The curves for the components are also depicted.

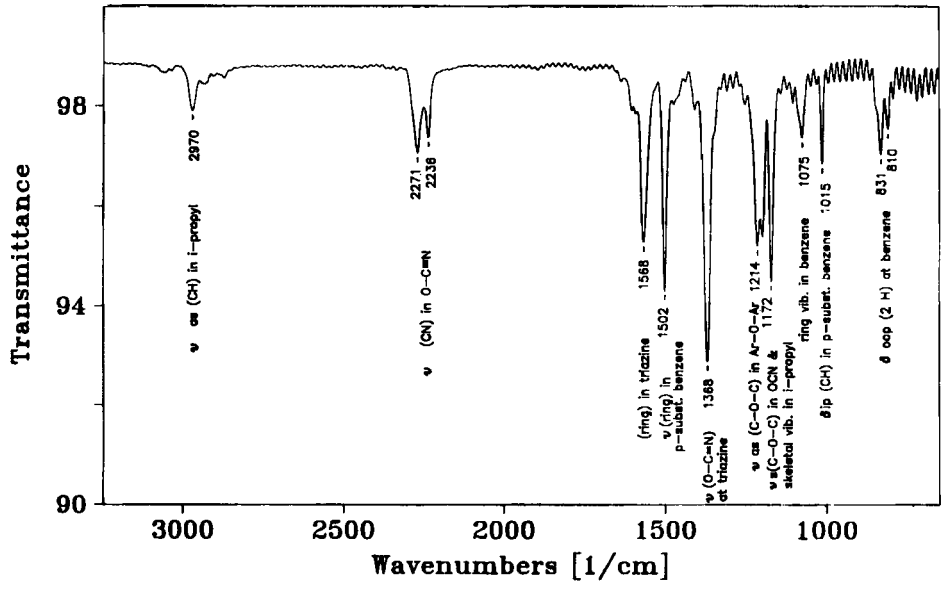

FIGURE 6 IR transmittance spectrum of a thick prepolymer layer on KBr pellet. Spectral resolution = 2 cm^{-1}.

Figures 7 a–c illustrate the topography of the prepolymer on silicon as it is seen by AFM. A 3 nm spin coating layer is shown in Figure 7a. The profile depth of the layer surface (determined by AFM) reaches just one tenth of the ellipsometric (mean) layer thickness. Hence, the coating is free of holes. It consists of prepolymer granules with ca 60–120 nm in diameter. The root mean square roughness is only twice that of the bare silicon wafer. A 2 nm dip coating film is shown in Figure 7b for direct comparison. The layer probably is also dense and, apart from additional high protrusions, consists of similar granules whose diameters amount to only 40–60 nm, growing only slightly for the thicker dip coating films. Due to the additional protrusions, the surface roughness is larger than for spin coating; however, it reduces to only twice the value of the bare wafer for films thicker than some 15 nm. Thicker spin coating films retain the smoothness and homogeneity of the thinner films as demonstrated by the 47 nm film in Figure 7c.

Things are quite different with the topography of the prepolymer on the aluminium substrate, Figures 8a–d. The 5.1 nm dip coating layer consists mainly of prepolymer agglomerations (white colour) with up to a few 100 nm in diameter. They concentrate in the valleys and around the peaks of the Al profile that can be clearly seen. Sometimes, the rich topographic structure makes it difficult to distinguish between prepolymer and aluminium substrate. The so-called "lateral force mode" for the AFM helps in that respect. This mode images a material contrast *via* some microscopic friction coefficient between AFM tip and sample surface. The Figure 8b compares the AFM contact mode image on the left with such a lateral force mode image on the right. The surface region is exactly the same for both images. For example, the two topographically similar features

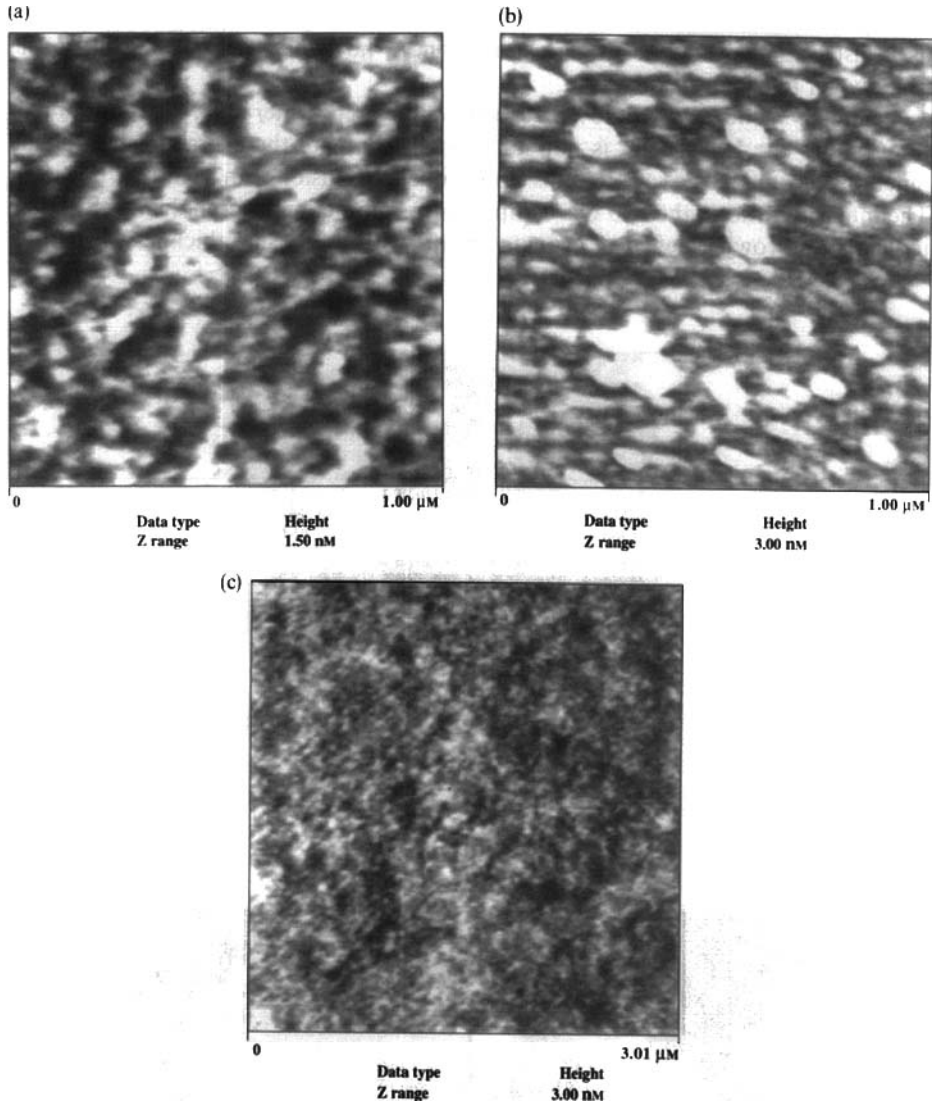

FIGURE 7 AFM images of prepolymer on silicon wafers. a) 3 nm spin coating, grey scale 1.5 nm, profile depth 0.3 nm, RMS roughness 0.29 nm; b) 2 nm dip coating, grey scale 3 nm, profile depth 0.5 – 2 nm, RMS roughness 1.6 nm; c) 47 nm spin coating, grey scale 3 nm, RMS roughness 0.33 nm.

on the left (arrows) are identified as a prepolymer agglomerate (bright) and as uncoated aluminium (dark) in the lateral force mode image on the right-hand side. Obviously, the thinnest dip coating films are not dense on aluminium. The same is true for the thinnest spin coating layers, Figure 8c. However, the prepolymer fills all substrate valleys with interconnected lakes. The prepolymer thickness has to be increased up to some 15 nm for obtaining dense layers on aluminium. Figure 8d provides the image of a 44 nm layer

as a last example. Despite the larger roughness, now the structure resembles the prepolymer films on silicon.

As already mentioned for the XPS spectra of the prepolymer bulk, the resolution of the Cls and the Nls spectra is not sufficient to compare the energetic state of the functional groups in the various films. Some other conclusions can be drawn, however. The intensity ratio of the two Ols components is a function of prepolymer thickness indicating a growing deficit of cyanate groups with decreasing thickness, Figure 9.

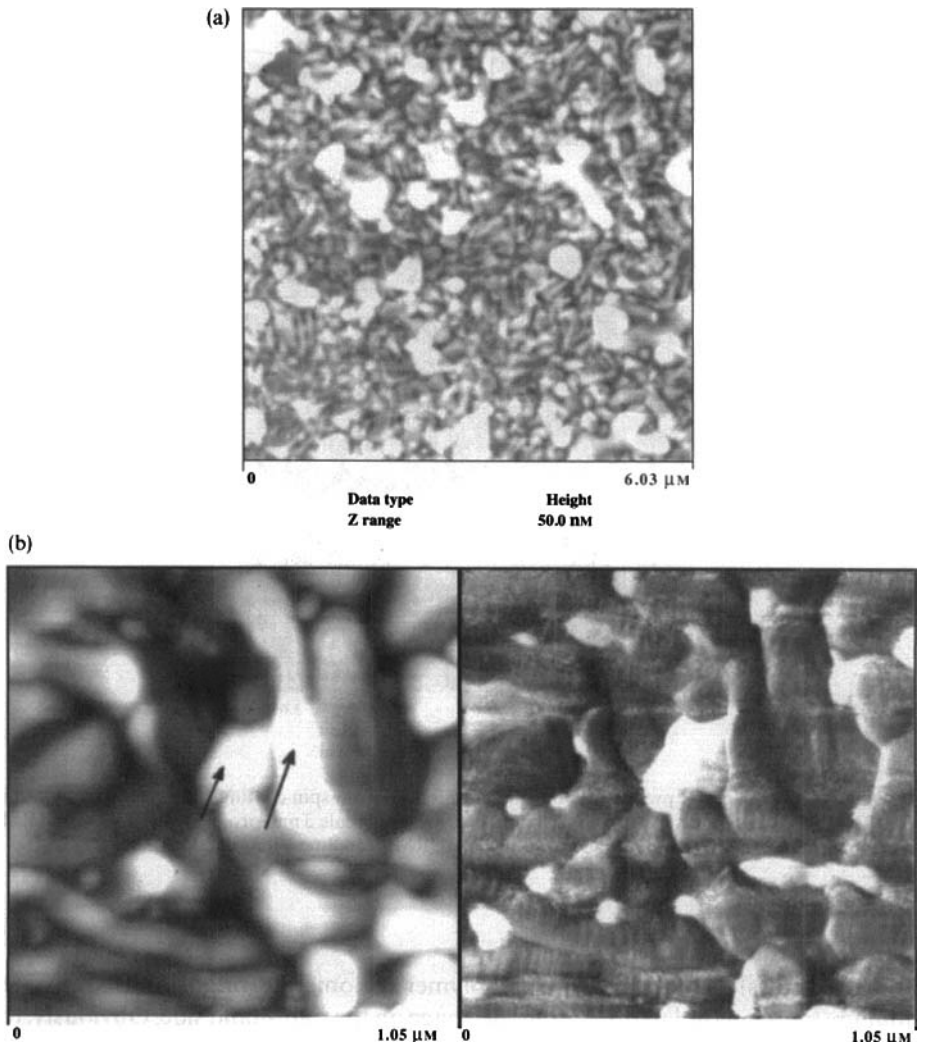

FIGURE 8 AFM images of prepolymer on the aluminium substrate. **a)** 5.1 nm dip coating, grey scale 50 nm, RMS roughness 8.9 nm; **b)** the same layer, topography (left, grey scale 25 nm), compared with the friction mode image (right) for the same sample area; **c)** 2 nm spin coating, grey scale 20 nm, RMS roughness 4.6 nm; **d)** 44 nm spin coating, grey scale 10 nm, RMS roughness 1.5 nm.

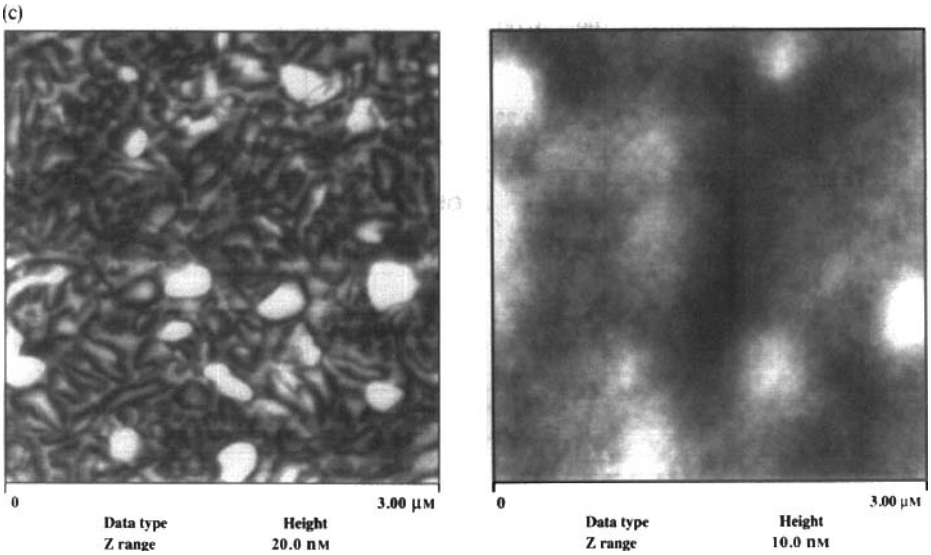

FIGURE 8 *(Continued).*

Generally, the ratio is less than the value of 2.23 that is expected from the molecular size distribution of the prepolymer. Storage experiments of samples in the UHV revealed that the deficit results to a considerable extent from a substantial monomer evaporation in vacuum. It should be noted that slight shifts of the photoelectron binding energies are detected for the prepolymer atoms on aluminium. Unfortunately, interference from the varying cyanate content, from the substrate oxide and from the carbon contamination hampers an identification of interphase interaction in that case. Since the prepolymer layers are dense and uniform on Si, they are suitable targets for angle-resolved XPS. Figure 10 provides the thickness dependence of the π-π^*-transition in the Cls spectrum which is characteristic for the benzene rings. The graph reveals an increase of concentration below ca. 10 nm. Hence, the concentration of triazine rings must be lower in the outer region of those prepolymer layers that has a thickness of approximately 1.5 nm in these measurements. Ten nanometers are only a few monolayers with respect to the dimensions of the trimer molecule. So we conclude that the triazine rings tend to enrich in the neighbourhood of the native silicon oxide by molecular orientation.

The infrared reflection spectra were taken with linearly polarized light on a FTS 60B (BioRad) with a SEAGULL reflection accessory (Harrick) and on a Nic 740 (Nicolet) combined with a Model 500 reflection unit (SPECTRATEC). Angle of incidence and polarization were chosen for maximum spectral intensity, that is p-polarization and 80° on aluminium substrates and s-polarization at 50° on silicon wafers. Figure 11 sketches the principles of external reflection IR spectroscopy. In many instances, a thin-film reflection spectrum differs from a transmission spectrum with respect to frequency position and band intensity. This may simply be due to anomalous dispersion caused by a strong variation of the refractive index of the coating, n_P, at a given absorption frequency.[12] These distinctions also depend on the angle of light incidence, Θ_i, and on

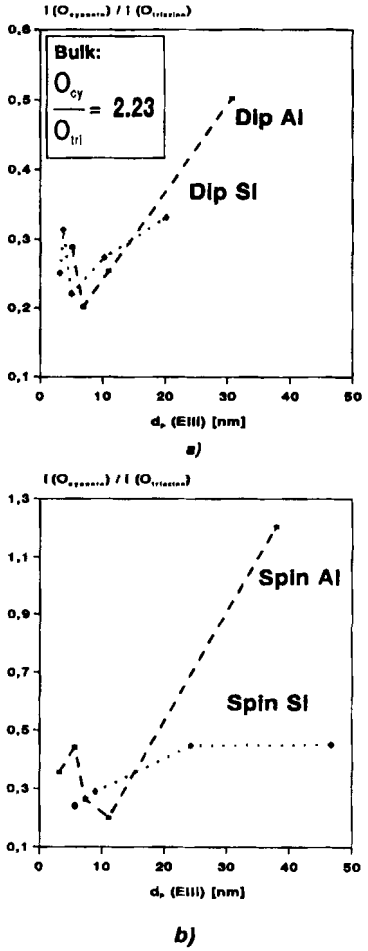

FIGURE 9 XPS Ols integral intensity ratio for the cyanate and the triazine components as a function of ellipsometrically-determined prepolymer film thickness on silicon and on aluminium. **a)** dip coating layers; **b)** spin coating layers.

the film thickness (absorption strength, respectively). Therefore, a straightforward interpretation of thickness effects in terms of intermolecular bonding or preferential molecular orientation can be misleading.

For this reason we adopted a different approach. This is to apply the bulk optical functions, n^*, of substrate,[13,14] oxide, [15,16] surrounding air and prepolymer (from the ATR spectrum), together with the corresponding thickness data, in a simulation of the IR spectrum for every sample. This spectrum would be found in the measurement if all parts of the sample had bulk properties. Therefore, it serves well as a reference in the discussion of the actually-measured reflection spectra. Figure 12 compares such a simulated bulk-like spectrum with the spectrum actually measured for a film on the aluminium substrate. At first glance, both spectra resemble very much the spectrum of the prepolymer bulk in Figure 6. Figures 13–16 depict the frequency position and the

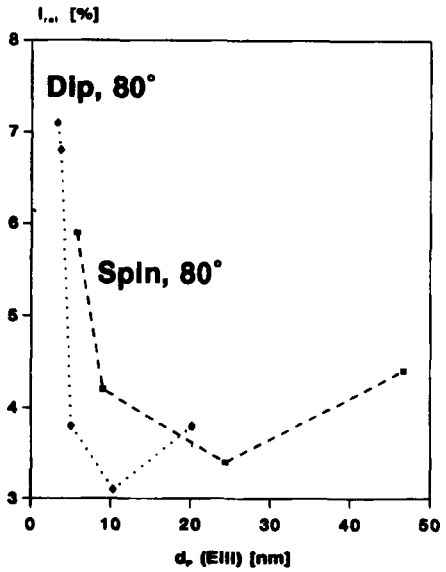

FIGURE 10 The π-π^*-transition in the Cls spectra of prepolymer on silicon as a function of film thickness. The photoelectron collection angle is 80°.

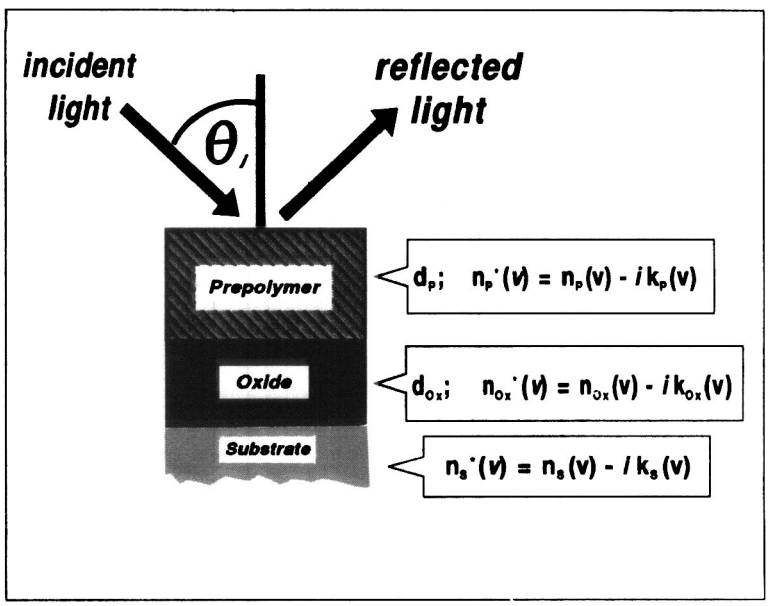

FIGURE 11 Principle of external reflection spectroscopy on layered systems.

relative intensity for selected bands as functions of prepolymer thickness in more detail. Figure 13 shows the band position of a (C ≡ N) stretching mode. No differences between simulation and measurement are observed, within the experimental error, either on aluminium or on silicon. The same is true for the other valence vibrations

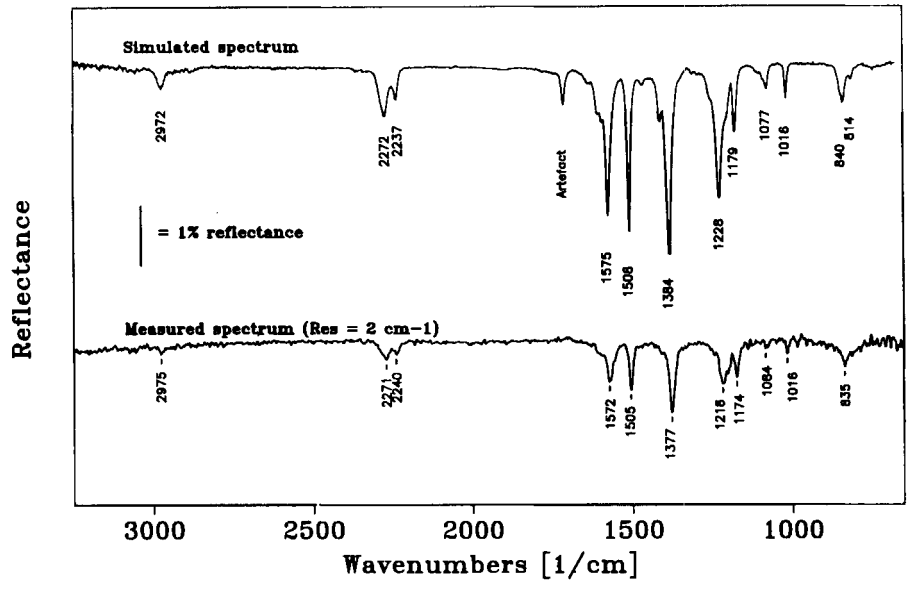

FIGURE 12 The simulated and measured external reflectance IR spectra for 7.4 nm thickness prepolymer spun onto aluminium substrate. $\Theta_i = 80°$, p-polarized light.

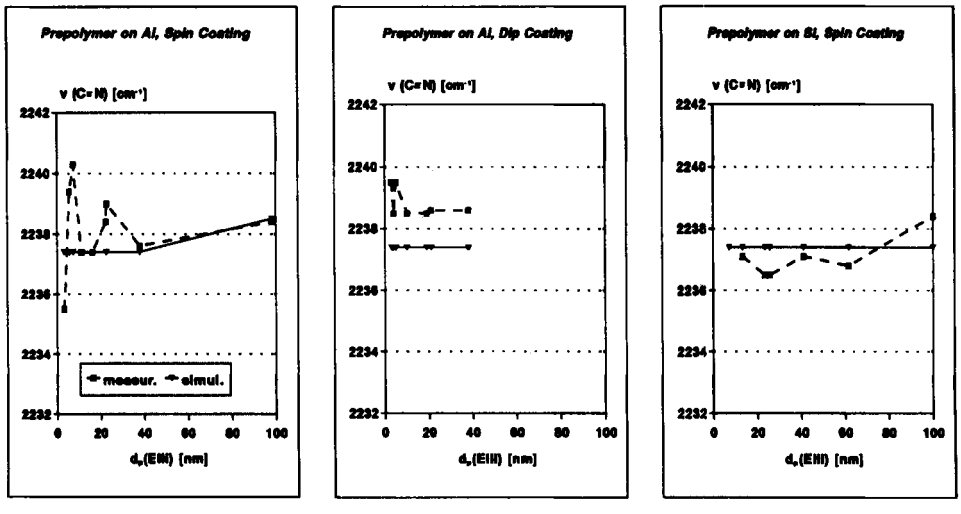

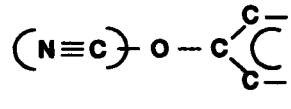

FIGURE 13 IR frequency of the (C ≡ N) stretching mode as a function of prepolymer thickness on aluminium and on silicon for spin and dip coating.

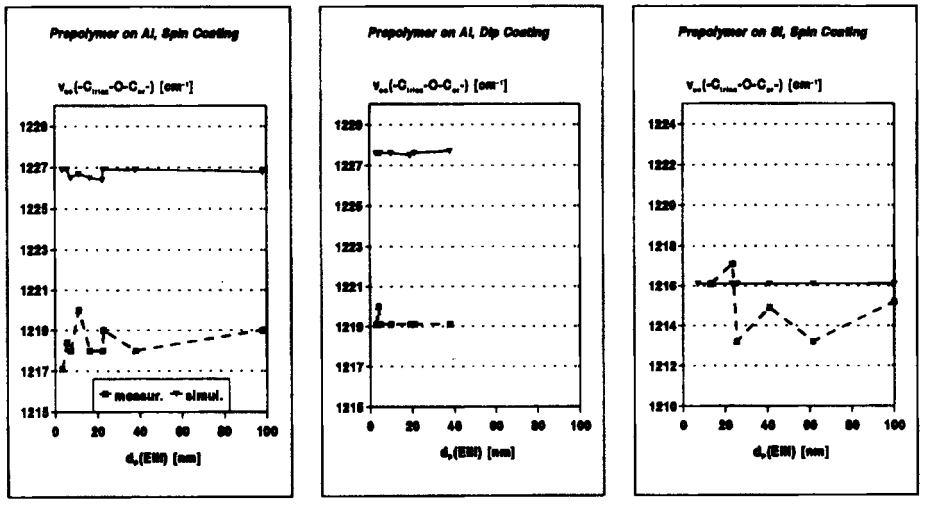

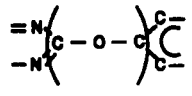

FIGURE 14 As in Figure 13 for the stretching mode of the oxygen bridge between the triazine and the benzene rings.

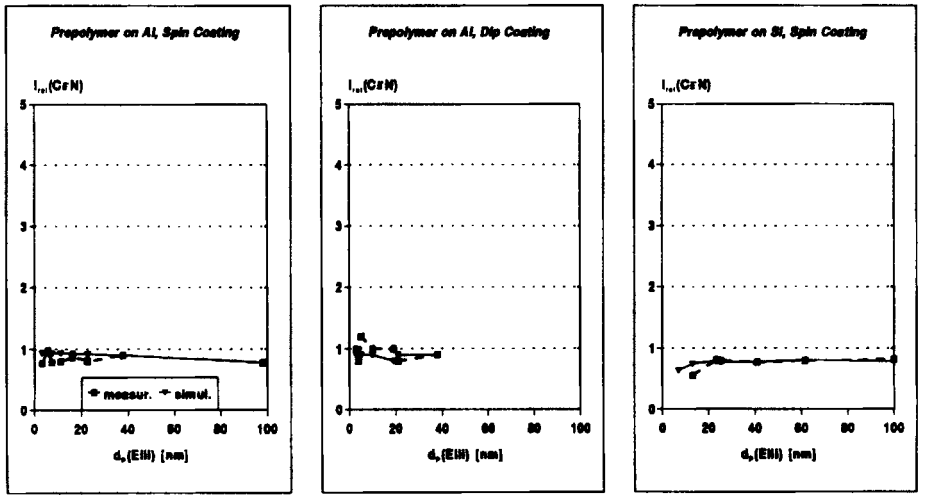

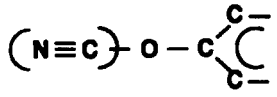

FIGURE 15 IR band intensity (relative to the peak height at 1016 cm^{-1}) for the (C ≡ N) stretching mode as a function of prepolymer thickness on aluminium and on silicon for spin and dip coating.

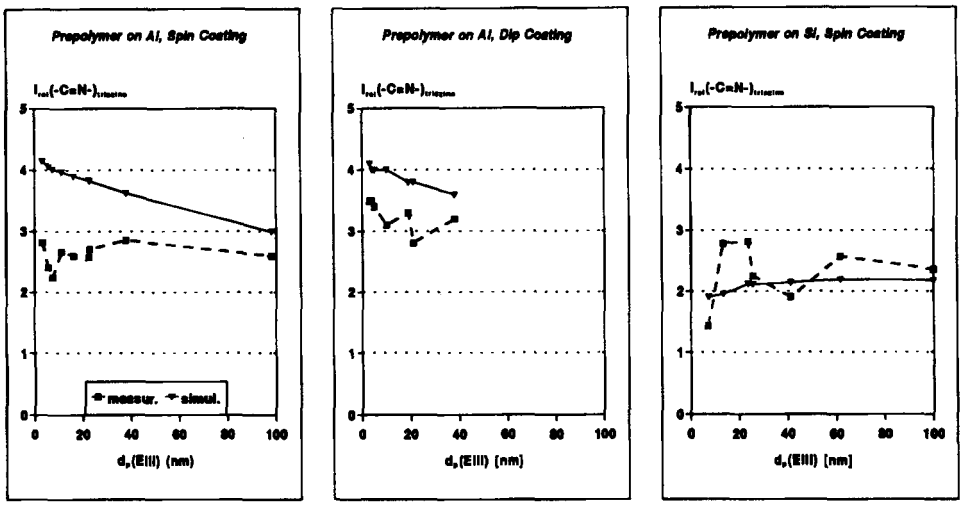

FIGURE 16 As in Figure 15 for the stretching mode of the oxygen bridge between the triazine and the benzene rings.

attributed to the cyanate group and to most of the other IR bands. That is good proof for the reliability of the utilized calculation procedures. Things are more interesting for the triazine grouping and its surroundings, Figure 14. On aluminium, their valence vibrations shift unambiguously to lower frequencies. The strongest shift, some 8 cm^{-1}, occurs for the oxygen bridge between triazine and benzene rings. The vibrations of $\nu(-N=C-O)$ and of $\nu(-N=C-)$ in the triazine and the vibration of the benzene ring (at *ca.* 1505 cm^{-1}) are also involved and lose between 2 cm^{-1} and 6 cm^{-1}. Surprisingly, all the frequency reductions extend over the entire thickness range up to 100 nm. They correspond to a very low energy loss of those molecular vibrations. For instance, 8 cm^{-1} corresponds to just 1 meV or *ca.* 0.7% of the vibration energy. No such frequency shifts occur for the prepolymer films on silicon! Therefore, it seems that the substrate causes the effect on aluminium. Common adhesion theories can hardly explain its long range, however.

Figure 15 compares the relative intensity of the $(C \equiv N)$ band as referred to an internal standard. The measurements reproduce the simulated data for all d_P-values and all samples. Hence, both concentration and orientation of cyanate groups in the prepolymer films are similar to the bulk. On the contrary, the experimental IR bands of $\nu(-C_{benzene}-O-C_{triazine}-)$ and $\nu(-N=C-)_{triazine}$ and of the benzene ring lose, on aluminium, more and more relative intensity with decreasing d_P as compared with the simulation. Figure 16 illustrates that behaviour for the $\nu(-N=C-)_{triazine}$ vibration in the triazine ring. The deviation clearly appears not only below 40 nm but extends over the whole thickness range. As the prepolymer composition does not change, that thickness dependence indicates a preferred orientation of triazine rings in a direction perpendicular to the plane of light incidence, *i.e.* parallel to the substrate surface. For

the silicon substrates, the measured data reproduce the simulated prepolymer bulk behaviour within the experimental scatter. Hence, the molecular orientation distributions on silicon are similar to the bulk for the considered film thickness interval.

DISCUSSION AND CONCLUSIONS

The combination of experimental methods described in this paper provides important information about the morphology and about the molecular state of ultra-thin organic coatings on solids.

Each method requires sophisticated tools for data processing. As a result, XPS and external reflection IR spectroscopy can reveal tiny changes in the energy and in the orientation of characteristic atomic groupings of the prepolymer molecules in the coatings just after preparation.

The Atomic Force Microscope shows structural details of the ultra-thin prepolymer films with characteristic lateral dimensions from some 10 nm up to a few micrometers. In particular, it reveals whether films are discontinuous or continuous.

Substrate flatness seems to be an important prerequisite for continuous organic layers. So the aluminium roughness of a few nanometers is sufficient to induce discontinuous films below about 10 nm mean thickness.

Up to now, our results show that the as-prepared prepolymer layers do not undergo serious chemical changes or pronounced adhesive interactions. The cyanate groups are not involved in specific interactions at all. The oxide on the silicon wafer is totally inert. The native aluminium surface induces changes in energy and orientation of the triazine rings. This may be considered as an indirect hint of some adhesive interaction of the cyanurate prepolymer with the aluminium substrate but the experimental facts do not explain the adhesion mechanism in detail yet. Moreover, the long range of the orientation effect could exert an influence on the network formation during the postcuring process. This might result in variations of the final mechanical properties in some interphase near the aluminium substrate.

To extend the picture, the effects of storage and the influence of the substrate state on the interphase deserve attention in further investigations. Moreover, in practical applications, the adhesive prepolymer formulation is cured. In view of the so far obtained results we expect that curing will not only complete the network but could also contribute to the final adhesive interactions.

Summing up, we consider both the advancements in analytical capabilities and the obtained experimental data as a good step forward in describing the physical and chemical state of polymer ultra-thin films on solids and the interphases between them. However, the construction of a physical model of that state is not simply done with the experimental facts only. We expect that molecular modelling will have to be added to the measurements in order to understand what the spectroscopic data tell us about the microscopic situation in the adhesive interphases.

Acknowledgements

This study is the result of research projects funded by the Volkswagen- Stiftung in Germany. We thank Mrs. S. Jährig for the valuable support by synthesizing the polymeric materials and Mr. H. Stuke for provision of

the aluminium substrates. It is also a pleasure to acknowledge the advice of Prof. M. Bauer in chemical synthesis.

References

1. D. A. Shimp, J. R. Christenson and S. J. Ising, *AroCy Cyanate Ester Resins: Chemistry, Properties and Applications*, Rhone-Poulenc Inc., Performance Resins & Coatings Div., 9800 E. Bluegrass Parkway, Louisville, KY 40299, USA.
2. J. P. Armistead and A. W. Snow, *Polym. Prepr.* **31**, 537 (1990).
3. D. A. Shimp, *Proc. 14th Meeting of the Adhesion Soc.* 16 (1991).
4. M. Bauer and J. Bauer, in *Chemistry and Technology of Cyanate Ester Resins*, I. Hamerton, Ed. (Blackie Academic & Professional, imprint Chapman & Hall, Glasgow, 1994), p. 58–86.
5. W. Brause, *Struktur- und H-Brückenbildungs- Untersuchungen an heterosubstituierten Nitrilen*, Thesis, p. 67–71, Zentralinst. Organ. Chemie, AdW der DDR, 1970.
6. V. A. Pankratov, V. V. Korshak, S. V. Vinogradova and A. G. Pucin, *Plaste und Kautschuk* **20**, 481 (1973).
7. G. Martin and R. Bacaloglu, *Organische Synthesen mit Cyansäureestern* (Akademie-Verlag, Berlin, 1980), pp. 33–35.
8. D. A. Shimp, J. R. Christenson and S. J. Ising, *Prepr. SPI- Epoxy Resin Formulators Division Conference*, Hollywood, Florida, USA, 1990.
9. Landolt Börnstein, *Zahlenwerte und Funktionen aus Physik, Chemie, Astronomie, Geophysik, Technik, I. Band "Atom-und Molekülphysik", 2. Teil "Molekeln I"* (Springer-Verlag, Berlin, Göttingen, Heidelberg, 1951).
10. H. J. Hediger, *Infrarotspektroskopie. Grundlagen, Anwendung, Interpretation*, in Bd. 11, von F. Hecht, R. Kaiser, E. Pungor and W. Simon, *Methoden der Analyse in der Chemie* (Akadem. Verlagsges., Frankfurt a.M., 1971).
11. G. Sokrates, *Infrared Characteristic Group Frequencies* (J. Wiley & Sons, Chichester, New York, Brisbane, Toronto, 1980).
12. M. K. Debe, *Progr. Surf. Sci.* **24 (1–4)**, 1 (1987).
13. M. A. Ordal *et al.*, *Appl. Optics* **24**, 4493 (1985).
14. D. E. Palik, Ed. *Handbook of Optical Constants of Solids* (Academic Press, New York, 1985).
15. V. Hopfe, *Erweiterung der Anwendungsbreite und Aussagefähigkeit optischs-pektroskopischer Untersuchungsmethoden für Festkörperoberflächen, Adsorbate und Schichtsysteme*, Thesis B, TU Chemnitz, 1984.
16. P. H. Gaskell and D. W. Johnson, *J. Noncryst. Solids* **20**, 153 (1976).